***Supporting Information for*:**

A Gauss's Law Analysis of Redox Active Adsorbates on Semiconductor Electrodes. The Charging and Faradaic Components of the Total Current Are Not Independent

Robert Vasquez,[1†] Jacob Waelder,[2†] Yifan Liu,[3] Hannah Bartels,[1] and Stephen Maldonado[1,2]

1. Department of Chemistry
   University of Michigan
   Ann Arbor, MI 48105-1055
2. Program in Applied Physics
   University of Michigan
   Ann Arbor, MI 48109-1055
3. Electrical Engineering and Computer Science
   University of Michigan
   Ann Arbor, MI 48105-1055

‡ These authors contributed equally to the completion of this work.

S1. Contents.

This document contains supporting information for the manuscript entitled "*A Gauss's Law Analysis of Redox Active Adsorbates on Semiconductor Electrodes. The Charging and Faradaic Components of the Total Current Are Not Independent"*. Section S2 summarizes the expressions for C_{sc}, C_{ss}, C_{surf}, and C_{elec}. Section S3 presents the tabulated values for the default conditions used to generate the calculated voltammograms and the quantitative features of the modelled voltammetric responses shown in the main text. Section S4 more explicitly comments on the information contained in asymmetry of the voltammetric responses. Section S5 presents details on the MATLAB code that was used to generate the figures in the main text. Section S6 lists the references cited within.

S2. Definitions of Differential Capacitances

The differential capacitances C_{sc}, C_{ss}, C_{surf}, and C_{elec} used in the model presented in the main text are described individually below.

Differential Capacitance of the Semiconductor Space Charge Layer, C_{sc} The derivative of the F_s function in *eq 9* defines the space charge capacitance, C_{sc}.

$$C_{sc} = \frac{\left(N_d \varepsilon_0 \varepsilon_{sc} k_B T\right)^{1/2} \frac{dF_s}{dE_{app}}}{\frac{d\left(\phi_{sc,b} - \phi_{sc,s}\right)}{dE_{app}}} \tag{S1}$$

The F_s function has multiple forms that depend on whether the semiconductor is in accumulation, depletion, or inversion.[1,2] In this work, we only consider accumulation and depletion conditions.

$$F_s = \left(e^{\frac{-q}{k_B T}\left|\left(\phi_{sc,b} - \phi_{sc,s}\right)\right|} + \frac{q}{k_B T}\left|\left(\phi_{sc,b} - \phi_{sc,s}\right)\right| - 1 \right)^{1/2} \tag{S2a}$$

$$F_s = \left(e^{\frac{+q}{k_B T}\left|\left(\phi_{sc,b} - \phi_{sc,s}\right)\right|} - \frac{q}{k_B T}\left|\left(\phi_{sc,b} - \phi_{sc,s}\right)\right| - 1 \right)^{1/2} \tag{S2b}$$

Eq S2a is operative in depletion and *eq S2b* applies in mild accumulation. *Eq S2b* must be further refined if $E_{app} << E_{fb}$.[3]

The two forms of C_{sc} that correspond to the depletion and mild accumulation cases, respectively, are presented below.[1]

$$C_{sc} = \frac{\left(\frac{q^2 N_d \varepsilon_0 \varepsilon_{sc}}{2 k_B T}\right)^{1/2} \left(1 - e^{\frac{-q}{k_B T}\left|E_{app} - E_{fb}\right| \frac{d\left(\phi_{sc,b} - \phi_{sc,s}\right)}{dE_{app}}}\right)}{\left(e^{\frac{-q}{k_B T}\left|E_{app} - E_{fb}\right| \frac{d\left(\phi_{sc,b} - \phi_{sc,s}\right)}{dE_{app}}} + \frac{q}{k_B T}\left|E_{app} - E_{fb}\right| \frac{d\left(\phi_{sc,b} - \phi_{sc,s}\right)}{dE_{app}} - 1 \right)^{1/2}} \tag{S3a}$$

$$C_{sc} = \frac{\left(\frac{q^2 N_d \varepsilon_0 \varepsilon_{sc}}{2 k_B T}\right)^{1/2} \left(e^{\frac{+q}{k_B T}\left|E_{app} - E_{fb}\right| \frac{d\left(\phi_{sc,b} - \phi_{sc,s}\right)}{dE_{app}}} - 1\right)}{\left(e^{\frac{q}{k_B T}\left|E_{app} - E_{fb}\right| \frac{d\left(\phi_{sc,b} - \phi_{sc,s}\right)}{dE_{app}}} - \frac{q}{k_B T}\left|E_{app} - E_{fb}\right| \frac{d\left(\phi_{sc,b} - \phi_{sc,s}\right)}{dE_{app}} - 1 \right)^{1/2}} \tag{S3b}$$

Eq S3a condenses to the so-called 'Mott-Schottky' expression[4,5] when 'E_{app}-E_{fb}' is sufficiently large to make the exponential terms negligible.

Differential Capacitance of Surface States, C_{sc} The derivative of the f_s function in *eq 10* of the main text yields the surface state capacitance, C_{ss}.

$$C_{ss} = \frac{qN_{ss}\dfrac{df_s}{dE_{app}}}{\dfrac{d\left(\phi_{sc,b}-\phi_{sc,s}\right)}{dE_{app}}} \tag{S4}$$

C_{ss} describes the storage of charge by trapping at a population of surface states. The exact form of f_s (and correspondingly C_{ss}) depends explicitly on the specific distribution of surface states within the semiconductor bandgap. In this work, we present the simplest case based on the Shockley-Read-Hall description of recombination at surface states. *Eq S5* describes C_{ss} for a semiconductor interface populated with monoenergetic surface states located at a potential '$E_{ss,fb,}$' that is referenced to the semiconductor flat band potential.[3,6]

$$C_{ss} = \frac{qn_i^2 S}{2N_d v} = \frac{qn_i^2}{2N_d v}\frac{k_{ss}N_{ss}\left(2+\dfrac{n_i}{N_{cb}}e^{\frac{q}{k_BT}\left(E_{ss,fb}-E_{cb,fb}\right)}+\dfrac{N_{cb}}{n_i}e^{\frac{-q}{k_BT}\left(E_{ss,fb}-E_{cb,fb}\right)}\right)}{\left(\left(\dfrac{n_i}{N_{cb}}e^{\frac{q}{k_BT}\left(E_{ss,fb}-E_{cb,fb}\right)}+\dfrac{n_i}{N_d}e^{\frac{q}{k_BT}\left(E_{app}-E_{fb}\right)\frac{d\left(\phi_{sc,b}-\phi_{sc,s}\right)}{dE_{app}}}\right)+\left(\dfrac{N_{cb}}{n_i}e^{\frac{-q}{k_BT}\left(E_{ss,fb}-E_{cb,fb}\right)}+\dfrac{N_d}{n_i}e^{\frac{-q}{k_BT}\left(E_{app}-E_{fb}\right)\frac{d\left(\phi_{sc,b}-\phi_{sc,s}\right)}{dE_{app}}}\right)\right)} \tag{S5}$$

In this description, C_{ss} is proportional to the surface recombination velocity, S, at the semiconductor interface. *Eq S5* follows the Shockley-Read-Hall description of S which is proportional to the density of surface states, N_{ss}, and the rate constant for trapping/de-trapping, k_{ss}. For simplicity, this work assumes the rate constants for electron and hole capture/release to/from the band edges are equivalent and large (10^{-8} cm^3 s^{-1}). Both considerations are reasonable assumptions with crystalline inorganic semiconductor electrodes.[6-8]

Differential Capacitance of the Surface Layer, C_{surf} The capacitance C_{surf} represents a 'parallel plate' capacitance. Unlike the other capacitance terms, C_{surf} is not potential-dependent and instead is only a function of the tether distance and the dielectric properties of the surface layer.

$$C_{surf} = \frac{\varepsilon_0\varepsilon_{surf}}{d} \tag{S6}$$

Differential Capacitance of the Electrolyte Diffuse Layer, C_{elec} The capacitance C_{elec} in *eq 17* in the main text is the familiar diffuse layer capacitance described by Gouy-Chapman theory.[9]

$$C_{elec} = \frac{d}{dE_{app}}\left(-\frac{2\varepsilon_0\varepsilon_{electrolyte}\kappa}{z}\frac{k_B T}{q}\sinh\left(\frac{z}{2}\frac{q}{k_B T}\left(\phi_{PET}-\phi_{sol}\right)\right)\right) = -\varepsilon_0\varepsilon_{electrolyte}\kappa\cosh\left(\frac{z}{2}\frac{q}{k_B T}\left(\phi_{PET}-\phi_{sol}\right)\right)\frac{d\left(\phi_{PET}-\phi_{sol}\right)}{dE_{app}} \quad (S7)$$

S3. Quantitative Features of Voltammetric Responses Shown in the Main Text

Table S1. Calculation Parameters for the Default Calculation Condition

Symbol	Units	Value
β	$Å^{-1}$	2
d	cm	$5.00x10^{-8}$
ε_0	Farads cm^{-1}	$8.85x10^{-14}$
ε_{sc}	--	11.7
ε_{surf}	--	3
ε_{elec}	--	33
λ	electron volt	0.6
$[A]_{s,0}$	mol cm^{-2}	$1x10^{-9}$(Figure 2), $1x10^{-10}$(Figures 3, 4)
$E_{cb,fb}$ - $E^0_{,fb}$	Volt	-0.3, -0.5
E_g	Volt	1.12
$E_{ss,fb}$ - $E_{cb,fb}$	Volt	-0.6
k_B	J K^{-1}	$1.38064852x10^{-23}$
$k_{et,max}$	cm^4 s^{-1}	$6.00x10^{-17}$
k_{ss}	cm^3 s^{-1}	$1.00x10^{-8}$
N_{cb}	cm^{-3}	$2.82x10^{19}$
N_d	cm^{-3}	$1.00x10^{17}$
n_{elec}	molec cm^{-3}	$6.022x10^{19}$
N_{ss}	cm^{-2}	$1.00x10^9$
N_{vb}	cm^{-3}	$6.54x10^{19}$
q	Couloumb	$1.60217662x10^{-19}$
T	Kelvin	298
v	Volt s^{-1}	0.1
z_A	--	2
z_{A-}	--	1
z	--	1

The peak current densities, potentials, mid-peak potentials, full-width-at-half-maxima, and peak splittings of the voltammetry shown in Figures 3 and 4 of the main text are tabulated below.

Table S2. Features in Voltammograms Calculated as a Function of Parameters that Affect the Space Charge Region, the Surface Layer, and the Diffuse Layer (Figure 3)

Voltammetric Feature[b,c]	$E^0 - E_{cb,fb}$ = Units	*Default Condition*[a]		*Change Diffuse Layer*		*Change Surface Layer*		*Change Space Charge Region*	
		-0.3 V	-0.5 V	-0.3 V	-0.5 V	-0.3 V	-0.5 V	-0.3 V	-0.5 V
		$n_{elec} = 10^{-1}$ M, $\varepsilon_{surf} = 3$, $N_{ss} = 10^{9}$ cm^{-2}		$n_{elec} = 10^{-5}$ M		$\varepsilon_{surf} = 1$		$N_{ss} = 10^{13}$ cm^{-2}	
$j_{p,c}$	μA cm^{-2}	1.102	1.333	0.855	1.071	1.022	1.238	1.040	1.247
$E_{p,c}$	V vs. E^0	-0.015	-0.163	0.027	-0.119	-0.012	-0.149	-0.013	-0.146
$j_{a,c}$	μA cm^{-2}	-0.757	-	-0.570	-	-0.815	-	-0.733	-0.871
$E_{a,c}$	V vs. E^0	0.009	-	0.058	-	0.009	-	0.013	0.089
$fwhm_c$	V	0.076	0.065	0.083	0.071	0.079	0.067	0.076	0.123
$fwhm_a$	V	0.119	-	0.133	-	0.110	-	0.111	0.104
$E_{1/2}$	V vs. E^0	-0.003	-	0.043	-	-0.002	-	0.000	-0.029
ΔE_p	V	0.024	-	0.031	-	0.021	-	0.026	0.235

a. the full set of parameters used in these calculations are listed in Table 2

b. subscripts '*c*' and '*a*' denote 'cathodic' and 'anodic', respectively; subscript '*p*' denotes value at peak

c. *fwhm* = full width at half maximum

Table S3. Features in Voltammograms Calculated as a Function of Redox Adsorbate Coverage (Figure 4)[a]

Voltammetric Feature[b,c,d]	Units	*'uncoupled'*	*'coupled'*		
		1.0×10^{-10} mol cm^{-2}	1.0×10^{-10} mol cm^{-2}	1.5×10^{-10} mol cm^{-2}	1.0×10^{-9} mol cm^{-2}
$j_{p,c}$	-	0.293	0.270	0.263	0.227
$E_{p,c}$	V vs. E^0	-0.016	-0.004	0.000	0.027
$j_{a,c}$	-	-0.202	-0.187	-0.183	-0.157
$E_{a,c}$	V vs. E^0	0.008	0.017	0.024	0.050
$fwhm_c$	V	0.075	0.081	0.082	0.086
$fwhm_a$	V	0.118	0.126	0.128	0.137
$E_{1/2}$	V vs. E^0	-0.004	0.007	0.012	0.039
ΔE_p	V	0.024	0.021	0.024	0.023

a. the full set of parameters used in these calculations are listed in Table 2

b. subscripts '*c*' and '*a*' denote 'cathodic' and 'anodic', respectively; subscript '*p*' denotes value at peak

c. *fwhm* = full width at half maximum

d. current densities are unitless (normalized)

S4. Information Contained in the Asymmetry of 'Coupled' Voltammetric Data

A useful but less obvious prediction from the presented framework is that the asymmetry in voltammetric data where the charging and faradaic current densities are coupled has information on the value of the flat band potential of the semiconductor, E_{fb}.

Figure S1 summarizes the point, where the specific parameter values used in the calculations are collected in Table S4. The conditions in Figure S1 correspond to voltammograms where the dimensionless time constant of the experiment (*'m'* in Table 1 of the main text)[10] is sufficiently large that the individual values of the forward and back rate constants are not controlling. That is, the function that describes the potential dependence of the fractions of *A* and A^- on the surface is the Fermi function, i.e. $\chi_A = \frac{1}{1+e^{\frac{q}{k_B t}\left(\gamma_{sc}+\gamma_{surf}\right)\left(E_{app}-E^0\right)}}$. Accordingly, 'Nernstian' (i.e. equilibrium) surface concentrations of *A* and A^- are maintained throughout the entire voltammogram.[10] In addition, the total concentration of redox adsorbate is sufficiently large to make C_F appreciable (as described in the main text). For reference, the x-axis in Figure S1 is the applied potential relative to the flat band potential, i.e. $E_{app} - E^0$, and the vertical dashed lines denote the position of E_{fb} on this scale. All parameters used to calculate the voltammograms in Figure S1 are held constant except the value of the standard potential of the redox adsorbate, i.e. $E^0 - E_{fb}$. In each plot, the solid line indicates the calculated voltammograms for 'coupled' behavior, as described in the main text.

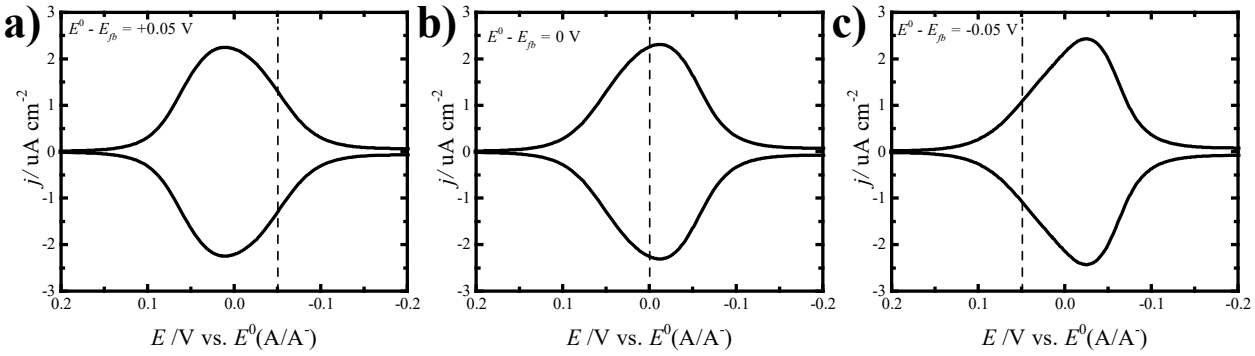

Figure S1. Comparison of the effect of the value of E^0 (indicated by the dashed vertical lines) relative to the E_{fb} on the apparent distortion caused in the voltammetric shape by 'coupling' of the faradaic and charging currents. The simulation parameters for these plots are listed in Table S3.

Figure S1a shows the calculated response expected when the standard potential of the redox adsorbate is more positive than E_{fb}. In this scenario, the 'coupled' response clearly exhibits asymmetry relative to the 'uncoupled' (i.e. symmetric) voltammetric response. The asymmetry in Figure S1a is skewed towards more negative potentials. Figure S1b highlights the case when the standard potential of the redox adsorbate is equal to E_{fb}. In this instance, the 'coupled' response again exhibits some perceptible asymmetry but towards negative potentials. Figure S1c illustrates the calculated response when the

standard potential of the redox adsorbate is more negative than E_{fb}. In this scenario, the semiconductor operates in mild accumulation for most of the voltammetric response. This statement means that *eqs S2b* and *S3b* are required but otherwise no other change is necessary to perform the presented treatment. In this case, the asymmetry is pronounced and directed towards more positive potentials because E_{fb} is now more positive than where the faradaic current passes.

In all cases in Figure S1, the peak current densities are not located precisely at E^0 because the apparent standard potential of the redox adsorbate shifts slightly when $\gamma_{elec} > 0$ (as described in the main text). Accordingly, care must be taken when abstracting information about the true standard potential of the redox adsorbate directly from such plots.

The trends regarding 'asymmetry' in Figure S1 can be interpreted as follows. C_{elec} decreases as the applied potential moves the semiconductor Fermi level towards E_{fb}. The corresponding diminution in C_{elec} enhances the 'coupled' behavior because the term $\frac{C_f}{(C_{sc}+C_{ss})C_{elec}}$ in *eq 31* of the main text (that describes the connection between the faradaic and charging currents) increases in magnitude as a result. Therefore, the asymmetry of the voltammetry that results from 'coupling' necessarily has information on the position of E_{fb} (as it pertains to where the faradaic current passes).

To be clear, the profile of the asymmetry in the 'coupled' voltammetry is sensitive to the potential dependence of C_{elec} but is not specifically an artifact of the Gouy-Chapman model. Neither the C_{sc} or C_{ss} functions are symmetric about E_{fb} either. So even if C_{elec} is described by a different model that is symmetric about E_{fb} (e.g. Helmholtz model), the denominator of the 'coupled' term in *eq 31* will not be symmetric about E_{fb}. Asymmetric voltammetry will still be expected when the faradaic and charging currents are 'coupled' but the shape of the asymmetry will change relative to what is shown in Figure S1.

Table S4. Parameters for Figure S1

Symbol	Units	Value
β	$Å^{-1}$	1
d	cm	5.00×10^{-8}
ε_0	F cm^{-1}	8.85×10^{-14}
ε_{sc}	--	11.7
ε_{surf}	--	6
ε_{elec}	--	80.1
λ	V	0.9
$[A]_{s,0}$	mol cm^{-2}	1.66×10^{-10}
$E_{cb,fb} - E^0_{,fb}$	V	-0.05, 0.00, +0.05
E_g	V	1.12
$E_{ss,fb} - E_{cb,fb}$	V	-0.6
k_B	J K^{-1}	$1.38064852 \times 10^{-23}$
$k_{et,max}$	cm^4 s^{-1}	6.00×10^{-17}
k_{ss}	cm^3 s^{-1}	1.00×10^{-8}
N_{cb}	cm^{-3}	2.82×10^{19}
N_d	cm^{-3}	5.00×10^{17}
n_{elec}	molec cm^{-3}	6.022×10^{20}
N_{ss}	cm^{-2}	1.00×10^{9}
N_{vb}	cm^{-3}	6.54×10^{19}
q	C	$1.60217662 \times 10^{-19}$
T	K	298
v	V s^{-1}	0.02
z_A	--	1
z_{A-}	--	0
z	--	1

S5. Description of and Instructions for MATLAB Scripts for Performing Calculations of the Capacitive and Faradaic Current-Potential Responses

Description The calculations were performed in two steps in MATLAB. Figure S2 graphically summarizes the workflow of the calculations for 'coupled' faradaic and capacitive currents.

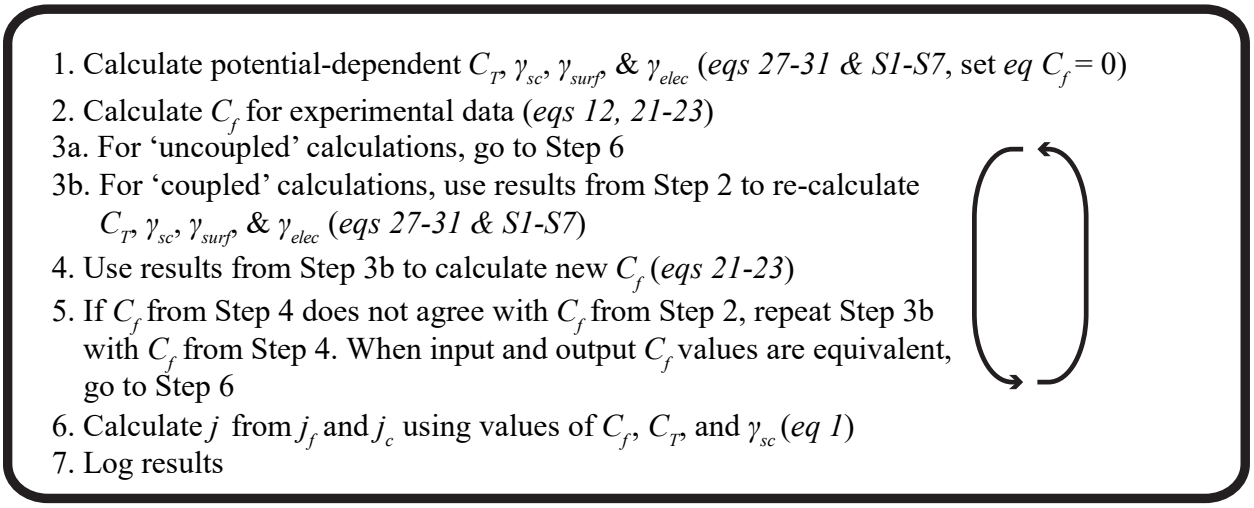

Figure S2. Visual description of the calculation steps used for 'uncoupled' and 'coupled' calculations.

First, arrays detailing the total electrode capacitance and the fractional potential drops across the semiconductor at every potential are generated by solving *eqs 27-31* of the main text, using all physically known/measureable parameters referred to in *eqs S1-S7*. Second, the faradaic current measured at every value of the applied potential is determined by using *eqs 12, 21*, *22*, and *23*. *Eqs 12, 21,* and *22* are specifically determined using the values of the fractional potential drops determined in the first step. For 'uncoupled' calculations, the total current is then determined using *eq 1*. For 'coupled' calculations, the initial faradaic current values are used to approximate C_f in *eqs 27-31* before calculating new values of the faradaic current. This process is repeated until the input and output faradaic current values match.

The total electrode capacitance, γ_{sc}, γ_{surf}, and γ_{elec} were determined by iteratively solving the relevant system of equations using the *vpasolve* function in MATLAB at every E_{app} value. The constraints for the calculations were the solved values had to be real numbers and all γ values were bound between 0 and 1. The tolerance and the default precision for *vpasolve* was 32 significant digits for all calculations.

Numerical integration was performed with the *integral* function in MATLAB rather than by simple trapezoidal rule. The former approach significantly cut down on the total calculation time. The *integral* function uses a global adaptive quadrature to significantly speed calculation time. The results were checked against integration performed with the trapezoidal rule and small (<0.001 V) potential steps. The results from the two integration method were generally indistinguishable. The default relative and absolute error tolerances of 1×10^{-6} and 1×10^{-10} were used throughout.

Evaluation of incomplete gamma functions was performed with the '*igamma*' function in the 'Symbolic Math Toolbox' of MATLAB. This method employs forward recursion to calculate a continued fraction that constitutes the incomplete gamma function.[11] We note there are several algorithms available in the literature for computing incomplete gamma functions.[12,13] As noted previously,[14] when *m* is sufficiently large, the values of incomplete gamma functions are large and difficult to compute operationally because of numerical overflow.[15,16] Whenever *m* was greater than 6, the reversible form of $\frac{d\chi_A}{dE_{app}}$ was implemented. Accordingly, the ability to distinguish very small differences in voltammograms that had reversible character was limited.

S6. References

1. Goldstein, M., *Semiconductor Surfaces*. John Wiley & Sons, Inc.: New York, 1965.
2. Lancaster, M.; AlQurashi, A.; Selvakumar, C. R.; Maldonado, S., *J. Phys. Chem. C* **2020,** *124* (9), 5021-5035.
3. Many, A.; Goldstein, Y.; Grover, N. B., *Semiconductor Surfaces*. John Wiley & Sons: Amsterdam, 1965.
4. La Mantia, F.; Habazaki, H.; Santamaria, M.; Di Quarto, F., *Russ. J. Electrochem.* **2010,** *46* (11), 1306-1322.
5. Cardon, F.; Gomes, W. P., *J. Phys. D: Appl. Phys.* **1978,** *11* (4), L63-L67.
6. Many, A., *J. Phys. Chem. Solids* **1959,** *8*, 87-96.
7. Yablonovitch, E.; Allara, D. L.; Chang, C. C.; Gmitter, T.; Bright, T. B., *Phys. Rev. Lett.* **1986,** *57* (2), 249-252.
8. Yablonovitch, E.; Swanson, R. M.; Eades, W. D.; Weinberger, B. R., *Appl. Phys. Lett.* **1986,** *48* (3), 245-247.
9. Bard, A. J.; Faulkner, L. R., *Electrochemical Methods: Fundamentals and Applications*. Second ed.; Wiley: New York, 2001.
10. Waelder, J.; Vasquez, R.; Maldonado, S., *J. Am. Chem. Soc.* **2022,** *144*, 6410-6419.
11. Kostlan, E.; Gokhman, D., *Internal Rep., Math. Dept* **1987**.
12. Abergel, R.; Moisan, L., *ACM Transactions on Mathematical Software* **2020,** *46* (1), 10:1-10:24.
13. Gautschi, W., *ACM Transactions on Mathematical Software* **1979,** *5*, 466-481.
14. Waelder, J.; Maldonado, S., *Anal. Chem.* **2021,** *93* (37), 12672-12681.
15. Gustafson, J. L.; Yonemoto, I. T., *Supercomputing Frontiers and Innovations; Vol 4, No 2 (2017)* **2017**.
16. Muller, J.-M.; Brunie, N.; Dinechin, F. d.; Jeannerod, C.-P.; Joldes, M.; Lefèvre, V.; Melquiond, G.; Revol, N.; Torres, S., *Handbook of Floating-Point Arithmetic*. Springer Nature: 2010.